PAPER

Fast three-dimensional micropatterning of PC12 cells in rapidly crosslinked hydrogel scaffolds using ultrasonic standing waves

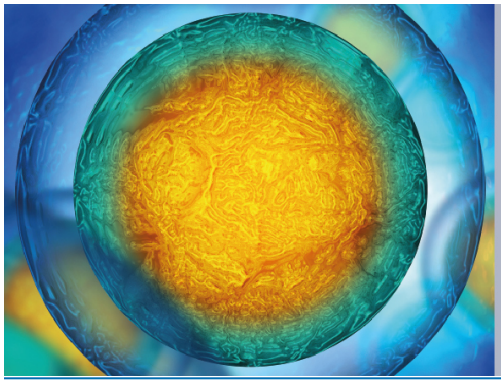

Biofabrication

PAPER

Fast three-dimensional micropatterning of PC12 cells in rapidly crosslinked hydrogel scaffolds using ultrasonic standing waves

Kai W Cheng[1,2,3], Layla Alhasan[1,2,5], Amgad R Rezk[2], Aswan Al-Abboodi[1,4], Pauline M Doran[1], Leslie Y Yeo[2] and Peggy P Y Chan[1,6]

[1] Faculty of Science Engineering & Technology, Swinburne University of Technology, Hawthorn, Australia
[2] Micro/Nanophysics Research Laboratory, RMIT University, Melbourne, Australia
[3] School of Applied Science, RMIT University, Melbourne, Australia
[4] Department of Biology, College of Science, University of Misan, Misan, Iraq
[5] Biology Department, Education College for Pure Sciences, Thi-Qar University, Iraq
[6] Author to whom any correspondence should be addressed.

E-mail: pchan@swin.edu.au

RECEIVED
10 April 2019

REVISED
6 October 2019

ACCEPTED FOR PUBLICATION
10 October 2019

PUBLISHED
2 December 2019

Keywords: tissue scaffold, nerve differentiation, hydrogel, cell alignment, micropatterning, standing waves

Supplementary material for this article is available online

Abstract

The ability to spatially organise the microenvironment of tissue scaffolds unlocks the potential of many scaffold-based tissue engineering applications. An example application is to aid the regeneration process of peripheral nerve injuries. Herein, we present a promising approach for three-dimensional (3D) micropatterning of nerve cells in tissue scaffolds for peripheral nerve repair. In particular, we demonstrate the 3D micropatterning of PC12 cells in a gelatin-hydroxyphenylpropionic acid (Gtn-HPA) hydrogel using ultrasound standing waves (USWs). PC12 cells were first aligned in 3D along nodal planes by the USWs in Gtn-HPA hydrogel precursor solution. The precursor was then crosslinked using horseradish peroxidase (HRP) and diluted hydrogen peroxide (H_2O_2), thus immobilising the aligned cells within 90–120 s. This micropatterning process is cost effective and can be replicated easily without the need for complex and expensive specialised equipment. USW-aligned PC12 cells showed no adverse effect in terms of viability or ability to proliferate. To our best knowledge, this is the first report on the effect of USW alignment on neural cell differentiation. Differentiated and USW-aligned PC12 cells showed directional uniformity after 20 d, making this technique a promising alternative approach to guide the nerve regeneration process.

1. Introduction

For decades, it has been recognised for many tissue engineering applications that three-dimensional (3D) scaffold-based culture is the preferred *in vitro* model over conventional two-dimensional (2D) culture because it possesses features that more closely resemble *in vivo* tissues [1, 2]. An ideal 3D scaffold is expected to mimic various aspects found *in vivo*, including physical, topographical, and geometrical features [3]. For example, a natural *in vivo* characteristic of organised tissue is the formation of bands of Büngner during the nerve regeneration process. These bands comprise linear assemblies of Schwann cells that proliferate along their axis of alignment and are essential for facilitating the reconnection of axons between nerve ends [4]. Accordingly, the ability to spatially arrange or manipulate the microenvironment and cell alignment in a tissue scaffold is widely accepted as a way to enhance the potential of scaffold-based tissue engineering applications. Recently, this has been enabled through microfabrication techniques, which allow the cell microenvironment to be tailored through controlled surface chemistry and topography.

In particular, microfabrication techniques such as photolithography [5, 6], soft lithography [7, 8], and current state-of-the-art 3D bioprinting [9–13] have been showcased to produce micropatterned structures or micropatterned cell arrangement in various tissue engineering studies. While these methods can achieve precise cellular arrangements, the fabrication steps involved are often complex and can require highly specialised equipment tailored to certain types of material. An alternative approach for cell patterning is to direct cellular movement by applying an external

force, which can be dielectrophoretic [14], optical [15], magnetic [16], acoustic [17], or combinations thereof [18].

Currently, nerve autograft remains the clinical gold standard treatment for peripheral nerve injuries; however it has several limitations such as donor site morbidity and loss of function at donor sites [19]. Short gaps between damaged nerves can be repaired with nerve guidance conduits, which are usually hollow tubes or nerve wraps, but these lack native *in vivo* features [20]. Over the years, many approaches have focused on integrating physical or topographical cues into biomaterials to promote the formation of Büngner bands with the aim of enhancing neurite outgrowth [21]. To name a few, electrospun biocompatible fibres [22–25], micropatterned surface grooves [26], and nanostructure patterned surfaces [27] have been widely reported in the literature as promising alternatives to conventional nerve conduits.

Here we explore a new, simple and cost-effective approach for spatially patterning cells directly within a 3D hydrogel system. Acoustic radiation forces associated with ultrasound standing waves (USWs) are used to invoke cellular spatial organisation. Previous biological applications of USWs that have been demonstrated with success over the years include cell sorting [28], cell trapping [29], cell mixing [30], and cell transfection [31]. In brief, the formation of a USW in a confined chamber results in both zero displacement planes and maximum displacement planes, namely the nodes and antinodes. The accompanying acoustic radiation forces vary depending on position relative to these planes. When cells/particles are subjected to USWs, they are aligned under these forces perpendicularly to the USW at half-wavelength intervals at either the nodes or antinodes depending on the density and compressibility of the particles relative to those of the surrounding medium [32–40]. Suspending the cells in a polymer solution that undergoes sol–gel transition ensures that the cells remain immobilised at fixed positions after removal of the acoustic signal. In the past, USWs have been demonstrated to align yeast cells in polyacrylamide [41], red blood cells and yeast cells in alginate and agar [42], and endothelial cells in collagen hydrogels [17, 43].

In our study, we set up a simple USW system comprising a cell chamber in contact with a lead zirconate titanate (PZT) disc as the acoustic source. We demonstrate the possibility of achieving simple and rapid immobilisation to fix the USW-aligned cells within the scaffold using gelatin-hydroxyphenylpropionic acid (Gtn-HPA) hydrogels. Previously developed by [44], Gtn-HPA hydrogels can be crosslinked by the oxidative coupling of HPA moieties catalysed by hydrogen peroxide (H_2O_2) and horseradish peroxidase (HRP). The gelation time can be easily tuned from seconds to 20 min by changing the concentration of HRP [45, 46]. Gtn-HPA hydrogel is biocompatible, biodegradable and have soft-tissue like mechanical properties; its gelatin based background contains Arg-Gly-Asp (RGD) peptides that serves as cell adhesive ligands. For example, Gtn-HPA hydrogels have been demonstrated to control neurogenesis and myogenesis of human mesenchymal stem cells [45], and has been demonstrated as brain tissue implants to attract neural progenitor cells migration [47]. For the first time, we demonstrate in this work a method to rapidly synthesize a 'gel block' of aligned cells in 90 s, taking advantage of the fast crosslinking rate of Gtn-HPA hydrogel. In this study, PC12 rat pheochromocytoma cells were used as a neuronal cell model. To our best knowledge, this is also the first report on aligning neural cells using USWs, and the first investigation of nerve differentiation of USW-aligned cells. We note, moreover, that the proposed system also serves as a generic, cost-effective platform that can be easily adopted for any tissue engineering study involving other cell types.

2. Materials and methods

2.1. Materials

Gelatin (Gtn, M_W = 80–140 kDa, pI = 5) and horseradish peroxidase solution (HRP, 100 units/mg) were purchased from Wako Pure Chemical Industries (Osaka, Japan). 3,4-Hydroxyphenylpropionic acid (HPA), N-hydroxysuccinimide (NHS), and 1-ethyl-3-(3-dimethylaminopropyl)-carbodiimide hydrochloride (EDC·HCl), phosphate buffered saline (PBS) were obtained from Sigma-Aldrich (Castle Hill, NSW, Australia). Dulbecco's Modified Eagle Medium (DMEM), horse serum (HS), fetal bovine serum (FBS), penicillin-streptomycin (PS), trypsin-EDTA, calcein AM, propidium iodide (PI), NP40 cell lysis buffer, Quant-iT™ PicoGreen® dsDNA Assay Kit, 4′,6-diamidino-2-phenylindole (DAPI), anti-rabbit Alexa-Fluor488 secondary antibody, and mouse nerve growth factor 7S (NGF 7S) were purchased from Life Technologies (Mulgrave, VIC, Australia). Tetramethylrhodamine- (TRITC-) conjugated phalloidin was obtained from Millipore (Merck Millipore, VIC, Australia). β-Actin, β-tubulin (TUBB), growth associated protein 43 (GAP-43), neurofilament-L (NF-L), dual specificity phosphatase 6 (DUSP6), and contactin associated protein 1 (Caspr1) markers were obtained from GeneWorks (Thebarton, SA, Australia). Aurum™ Total RNA Mini Kit, iScript™ cDNA Synthesis Kit, and SsoAdvanced™ universal SYBR® Green Supermix were purchased from Bio-Rad Laboratories (Gladesville, NSW, Australia). Rabbit anti-β-tubulin, rabbit anti-synapsin I, and rabbit anti GAP-43 primary antibodies were purchased from Abcam (Cambridge, MA, USA). Fluoresbrite YG carboxylate microspheres were acquired from Polysciences (Warrington, PA, USA).

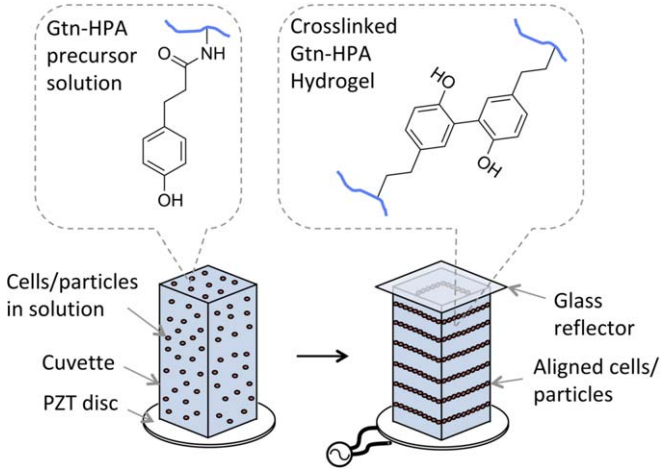

Figure 1. Schematic depiction of the setup for USW alignment of particles and cells in a cuvette.

2.2. Cell culture

PC12 cells (CellBank Australia, Westmead, NSW, Australia) were grown and maintained in a 37 °C, humidified 5% CO_2 incubator for up to 20 passages with complete medium consisting of DMEM supplemented with 10% HS, 5% FBS, and 50 units/ml PS. For differentiation studies, the complete medium was replaced with differentiating medium containing DMEM supplemented with 1% HS, 80 ng ml^{-1} NGF^{-} 7S, and 50 units ml^{-1} PS.

2.3. USW system setup and characterisation

The USW experimental setup (figure 1) consisted of a sample chamber, a 1.5 cm diameter lead zirconate titanate (PZT) disc (Fuji Ceramics Corporation, Shizuoka-ken, Japan) as the acoustic source, and a glass slide as the acoustic reflector. The sample chambers were either 10 × 25 × 10 mm (W × H × D) cuvettes or 12 × 25 mm (ø × H) glass tubes. USWs were generated by applying an electrical signal to the PZT using a signal generator (N9310, Agilent Technologies, Mulgrave, VIC, Australia) and an amplifier (ZHL-1-2W, Mini-Circuits, Brooklyn, NY, USA). The working frequency of the device was maintained in the range 2.15–2.25 MHz corresponding to the resonance frequency of each PZT disc verified using a vector network analyser (ZNB4, Rohde & Schwarz, Munich, Germany).

USW alignment was first characterised using fluorescent microspheres. Images were acquired using either a handheld digital microscope (AM4113-FVT, Dino-Lite Digital Microscope, New Taipei City, Taiwan), or a digital single lens reflex camera (D600, Nikon Instruments, Melville, NY, USA) with long-distance microscope attachment (K2/S2, Infinity Photo-Optical Company, Boulder, CO, USA). Images were then imported to ImageJ (National Institutes of Health, Bethesda, MD, USA) for fast Fourier transform (FFT) analysis. The area inside the cuvette that excluded the wall of the cuvette was selected as the region of interest in the analysis.

2.4. Simultaneous cell alignment and encapsulation in Gtn-HPA hydrogel

Gtn-HPA conjugates were synthesised using the process described in [44]. Lyophilised Gtn-HPA was first dissolved in complete medium to give a final concentration of 3 wt%. PC12 cells were subsequently suspended in the Gtn-HPA solution at a concentration of 2.4 × 10^6 cells ml^{-1}. 2.5 ml of the cell-containing Gtn-HPA solution was then transferred to the cuvette. 9 μl of HRP and 8.5 μl of 1% H_2O_2 were added to the solution to give final concentrations of 0.09 units ml^{-1} and 1.09 μM, respectively. The mixture was then quickly mixed by pipetting for approximately 10 s with a 1000 μl pipette before covering the cuvette with a glass slide. At this point, the cells in the chamber were subjected to the USW by turning on the signal generator and amplifier. The electrical signal was maintained for approximately 90 s to allow complete Gtn-HPA gelation. The gelated 'cell block' was then transferred to a tissue culture plate and maintained in complete medium for further experiments. The gelation time of the Gtn-HPA hydrogel was determined using the inverted tube method according to Gupta *et al* [48] in a separate experiment (supplementary materials are available online at stacks.iop.org/BF/12/015013/mmedia).

The morphology of the aligned cells was visualised using optical microscopy. To estimate the peak-to-peak distance between aligned rows of cells, a line perpendicular to the cell bands was drawn on the microscopy images and the greyscale intensities of each pixel along the line was obtained using ImageJ. The cell bands and the background hydrogel each have different optical properties therefore giving rise to different greyscale intensities along the line. The measurement was repeated for multiple samples. Control

samples were prepared using the same procedures as above but without USW exposure.

2.5. Cell viability and proliferation assays

To estimate cell viability as well as to visualise the morphology of the cells 24 h after USW exposure, the cell-containing hydrogel was stained with calcein AM followed by PI according to the manufacturers' instructions. The stained samples were then visualised using a laser scanning confocal microscope (LSCM; A1, Nikon Instruments, Melville, NY, USA).

To quantify the effect of the input electrical power on cell viability, cell-laden hydrogels were prepared using USWs with different input powers (0–1.17 W). After further culture in hydrogel for 24 h, the cells were released by degrading the hydrogel using 0.25% trypsin-EDTA for 2 h, followed by staining with calcein AM and PI. The numbers of live and dead cells were then quantified using flow cytometry (Accuri C6, BD Biosciences, North Ryde, NSW, Australia).

The effect of USW exposure on the PC12 cells' ability to proliferate was also investigated. After exposure to USW, the cell-containing hydrogels were cultured in complete medium that was rich in serum but contained no NGF. Cell proliferation in the hydrogel post-USW alignment was determined by quantifying DNA using a PicoGreen® assay kit according to the procedure documented in [49]. In brief, the cells were released from the hydrogel at days 1, 3, 5, and 7. These were then washed twice with cold PBS, centrifuging for 5 min at 1200 rpm after each wash. The collected cell pellet was lysed on ice for 30 min in 100 μl of NP40 cell lysis buffer with vortexing every 10 min. The clear lysate was collected after centrifuging the mixture at 13 000 rpm for 10 min at 4 °C. 100 μl of PicoGreen® reagent was added to the clear lysate and incubated for 5 min in the dark at room temperature. Finally, the fluorescence was measured using a multi-mode microplate reader (SpectraMax Paradigm, Molecular Devices, Sunnyvale, CA, USA) at an excitation wavelength of 480 nm and emission wavelength of 520 nm. The number of cells in the sample was determined by comparing fluorescence readings with a standard curve constructed using a set of cell lysates generated using a known number of cells.

2.6. Cell differentiation and gene expression (qPCR)

The effect of USW exposure on the PC12 cells' ability to differentiate was investigated as a separate experiment. To differentiate the PC12 cells, after USW alignment, the hydrogel with encapsulated cells was transferred to a well plate containing differentiating medium. Spent medium was exchanged with fresh differentiating medium containing NGF and low serum every alternate day. Gene expression for the differentiated PC12 cells was quantified by quantitative real-time polymerase chain reaction (qPCR) using the markers listed in table 1 (GeneWorks, Thebarton, SA, Australia). After 10, 15, and 20 d of differentiation, cell-containing scaffolds were digested in 0.5% trypsin-EDTA for 1 h. Ribonucleic acid (RNA) was then extracted from the collected cell pellets with an Aurum™ Total RNA Mini Kit according to the manufacturer's instructions. The RNA quality and concentration were measured using a spectrophotometer (Optizen NanoQ, Mecasys, Daejeon, South Korea). Complementary DNA (cDNA) was synthesised from the isolated RNA using the iScript™ cDNA Synthesis Kit. qPCR analysis was performed using a Biorad CFX96 PCR system (Biorad, Gladesville, NSW, Australia) with SsoAdvanced™ universal SYBR® Green Supermix. After 300 s of denaturation at 95 °C, 40 PCR cycles were performed at 94 °C for 15 s, 58 °C for 20 s, and 72 °C for 25 s. The mRNA levels were normalised to those of β-actin. Changes in gene expression were calculated as fold changes using the $\Delta\Delta$Ct method [50].

2.7. Immunocytochemistry

For an immunocytochemistry study at day 20 of the differentiation culture, the hydrogels with encapsulated cells were first fixed with 4% paraformaldehyde for 1 h at room temperature, followed by an hour of incubation at room temperature in blocking buffer containing 1% bovine serum albumin in PBS. The hydrogels were incubated with the following primary antibodies for 48 h at 4 °C: rabbit anti-β-tubulin, rabbit anti-synapsin I, and rabbit anti GAP-43. The samples were then labelled by incubating the cell embedded hydrogel with anti-rabbit AlexaFluor488 secondary antibody for 24 h, followed by incubation for 1 h in TRITC-conjugated phalloidin at room temperature in the dark. All antibodies were diluted according to the manufacturers' instructions. Finally, cell nuclei were counterstained with 1:1000 DAPI for 15 min The samples were washed with PBS between each staining step (3 $\times$ 5 min). Confocal images of the cells were then acquired using confocal laser microscopy.

2.8. Quantification of neurite alignment

In order to assess neurite alignment, the orientation angle of neurite outgrowth with respect to the cell bodies of individual cells was determined using a method modified from Standley *et al* [55]. Confocal images from the immunocytochemistry study were analysed using ImageJ. In brief, a reference line was drawn in each image; cells were first selected randomly from each image, and an axis parallel to the reference line was drawn on each cell body. A second line was drawn parallel to the direction of neurite outgrowth on each cell. The orientation angle of neurite outgrowth with respect to the cell body axis of individual cells was measured. For each image, the standard deviation of all orientation angles was calculated. The measurement was performed for both USW-treated

Table 1. qPCR primer sequences and associated references.

Primer	Sequence (5′-3′)	Size (bp)	References
β-actin	Forward: GTTGACATCCGTAAAGACC Reverse: TGGAAGGTGGACAGTGAG	200	[51]
TUBB	Forward: TCACTACAGCATGGGAGCAG Reverse: TGAATTGCTTTAATGGTGGTATC	128	[52]
GAP-43	Forward: GAGGGAGATGGCTCTGCTAC Reverse: CACATCGGCTTGTTTAGGC	240	[51]
NF-L	Forward: GTTGGGAATAGGGCTCAATCT Reverse: CCAGGAAGAGCAGACAGAGGT	280	[53]
Caspr1	Forward: TGACTCTGAACTTGGAGGGTCGTG Reverse: TATAGCGCATCCATGTGCCAGTCT	219	[54]

samples and control (untreated) samples; a total of 50 standard deviation measurements were made for each group.

2.9. Statistical analysis

All experiments were conducted with at least three replicates. The results are reported as an average value $\pm$ standard deviation. One-Way Analysis of Variance (ANOVA) was used to compare multiple groups of data. The Student *t*-test was used to compare two groups of data. Differences were considered statistically significant when $p < 0.05$.

3. Results and discussion

3.1. Alignment characterisation

When confined particles or cells are exposed to USWs and subjected to the primary acoustic radiation force associated with USWs, bands of aligned cells form instantly at the pressure nodal planes. Within minutes, these bands thicken and shorten due to secondary acoustic radiation forces [31]. Unless arrested in their positions, the cell bands or alignment patterns eventually collapse and disperse when the body force of the cell agglomerates exceeds the acoustic radiation force as illustrated in the supplementary materials. Such phenomena was also observed and explained by Lee & Peng [31]. To immobilise the cell alignment bands before their collapse, a suspending medium that can be easily solidified within minutes is preferred. It is for this reason that Gtn-HPA hydrogel was selected as the 'fixation' medium due to its versatility in terms of its tunable gelation rate and soft-tissue-like properties. The gelation time of Gtn-HPA hydrogel is dependent on the concentration of HRP, while its stiffness can be varied by adjusting the H_2O_2 concentration [44]. Such flexibility in tuning of the gelation time, makes Gtn-HPA extremely useful when coupled with USW cell trapping, given that some drift can occur over time [31], leading to smearing of the alignment patterns. In this work, the concentration of HRP was optimised to keep the gelation time within a window of 90–120 s. We found that this time frame was sufficient for gelation to occur whilst 'fixing' most of the cell bands in place.

We also note that a condition for the cell alignment within the chamber is that the attenuation length of the sound waves in the media at the frequency used is much greater than the dimensions of the chamber such that the sound waves penetrate across the entire containment. In other words, a standing wave is formed when the sound waves propagate all the way to the opposing boundary and reflect so that the transmitted and reflected waves superimpose to set up a standing wave.

Alignment patterns can be altered with chambers of different geometry due to the nature of the acoustic wave reflection off the side walls of the chamber, giving rise to different standing wave patterns. For example, figure 2(a) shows the side view of the linear patterns of fluorescent particles that form under when USWs are applied to the square cuvette. Figure 2(b), on the other hand, shows the top view of radial patterns arising in a circular tube. These representative images show that the alignment patterns are critically dependent on the boundary conditions (i.e. the walls and hence the geometry of the containment) due to the reflection of the sound waves that set up the standing waves along which the cells are trapped and hence align. Both figures 2(c) and (d) show the FFT images corresponding to each alignment pattern, indicating the regularity of the patterns. These results are qualitatively representative of the entire hydrogel volume irrespective of the position along the same axis that the two-dimensional planar cross-sectional cut was acquired, thus providing a degree of confidence that regular 3D patterning can be achieved throughout the entire system volume.

Such ability to align cells in 3D with different patterns can be useful for mimicking different types of tissue, therefore highlighting the flexibility of the technique. For example, it offers the potential to mimic muscle tissue in which endothelial cells are known to orient in the direction of their longitudinal axis [56], or to mimic aortic valve leaflets in which the thinner tissues are known to align in the radial direction [57].

Figure 3(a) shows a representative image of bands of immobilised PC12 cells in hydrogel obtained at

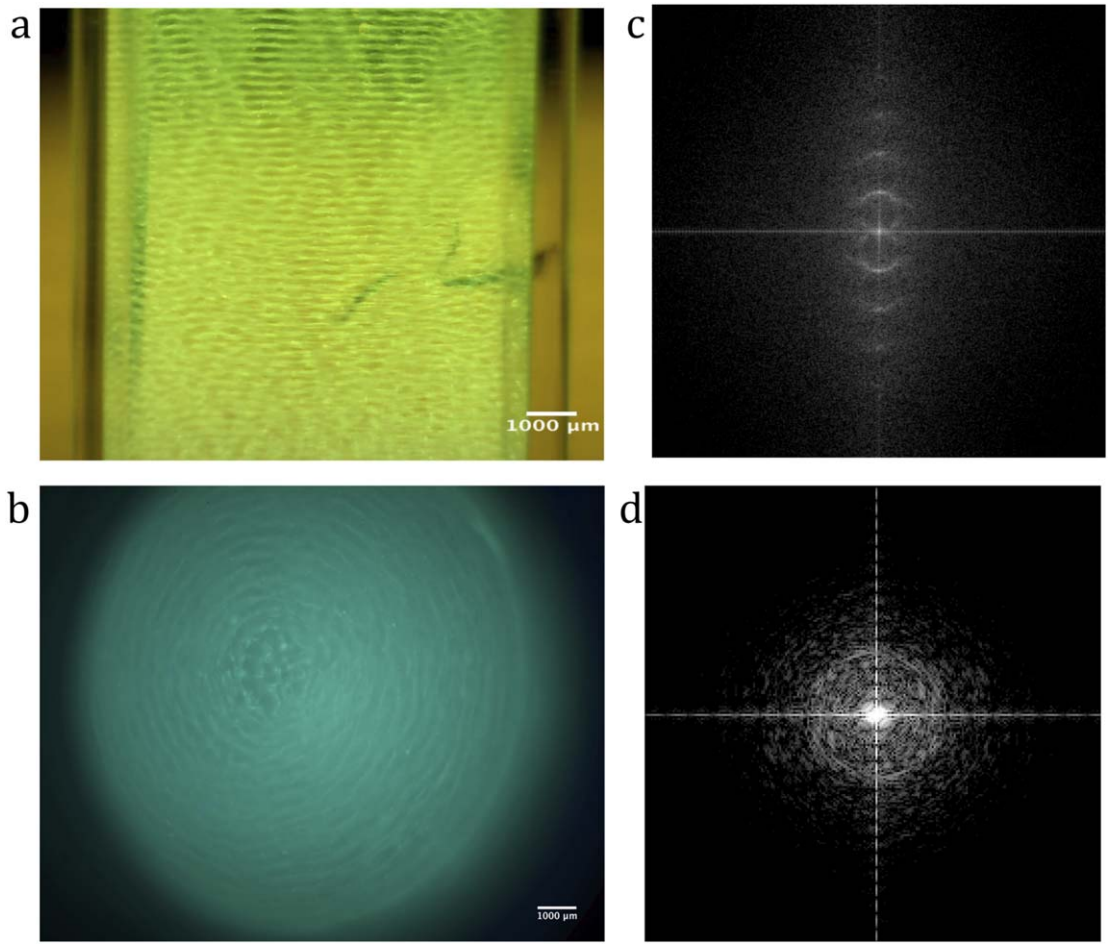

Figure 2. Alignment of fluorescent particles under USWs in chambers of different geometry. (a) Side view of the patterns in a square cuvette. (b) Top view of the patterns in a circular tube. (c) and (d) show FFT images corresponding to the patterns in (a) and (b), respectively. Scale bars represent 1000 μm lengths.

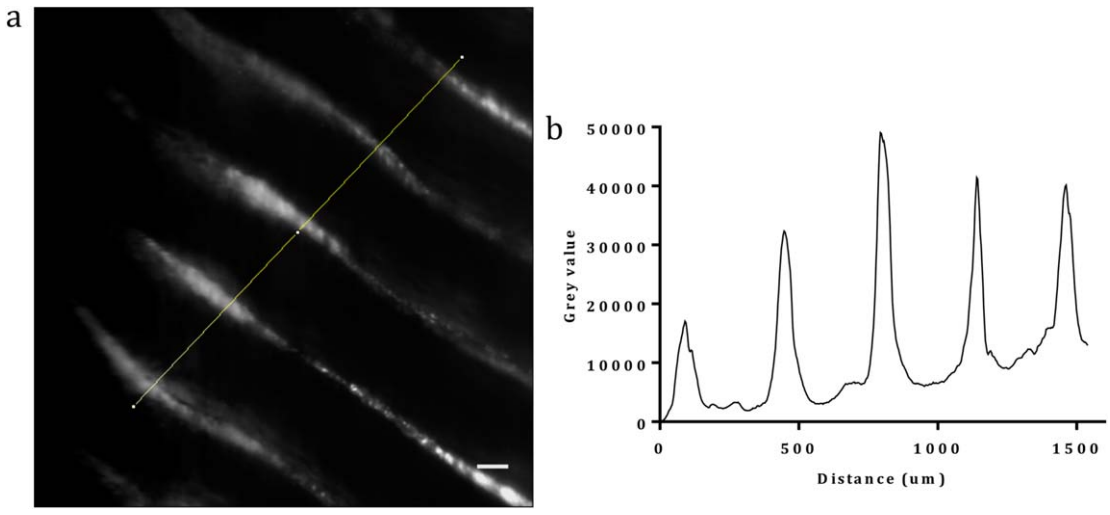

Figure 3. (a) Representative image showing aligned PC12 cells encapsulated in Gtn-HPA hydrogel at an applied USW power of 0.45 W. The scale bar denotes 100 μm. (b) Profile showing the distribution of greyscale intensity associated with pixels along the line shown in (a).

2.18 MHz. Figure 3(b) shows the distribution of cell bands within the hydrogel. The *x*-axis represents the distance along the line drawn in figure 3(a), while the *y*-axis captures the greyscale intensity associated with the pixels in the image along that line. The peaks therefore correspond to the location of the cell bands where

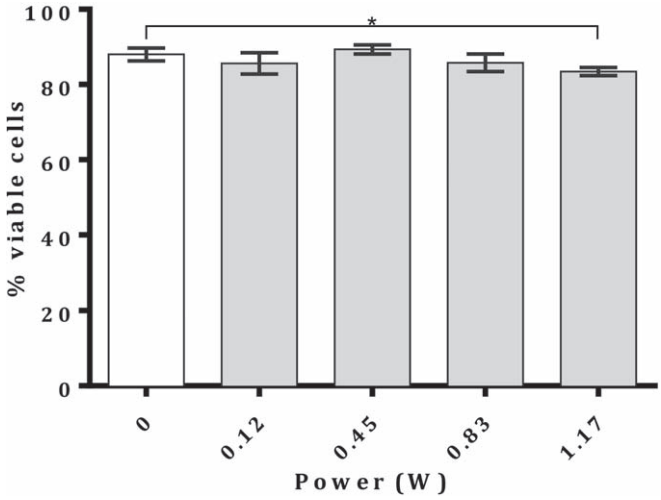

Figure 4. Viability of PC12 cells in the hydrogel determined by flow cytometry 24 h after USW alignment as a function of the input power. The first bar on the left represents the control with no USW treatment. Data are shown as a mean value ± standard deviation ($^{*}p < 0.05, n = 3$).

the value of the pixel greyscale intensity arises from the contrast of the concentrated cell bands relative to the image background. The half-wavelength separation distance (cell banding) ($\lambda/2$) can be estimated as $\lambda/2 = c/2f$, where c is the velocity of sound in water (taken as 1.48 km s^{-1} [32]) and f is the working frequency. Therefore, for f in the range 2.15–2.25 MHz, the half-wavelength separation distance was estimated at approximately 329–345 μm. The average peak-to-peak distance was estimated to be ~343 ± 15 μm, which relates closely to the theoretical separation distance specified by the half-wavelength of the USW.

3.2. Cell viability and proliferation

In our experiments, the threshold power for initiation of PC12 cell alignment was 0.12 W. Beyond 1.17 W, a recirculating flow known as acoustic streaming [58] was observed. The intensity of acoustic streaming increased as the power applied was increased, dispersing the cells away from the nodal planes and hence disrupting the cell bands. Accordingly, for cell aggregation experiments, the input power was limited to a window of 0.12–1.17 W.

Cells were released from the hydrogel 24 h after USW alignment and immobilisation for subsequent analysis by flow cytometry. Figure 4 shows the number of viable cells as a function of the power applied to the USW system. With the exception of 1.17 W ($p < 0.05, n = 3$), there was no significant difference in terms of viability between the USW-aligned cells and control cells that were not exposed to ultrasonic excitation. Similar results were reported by Garvin *et al* [17] who did not observe any damage to the cells in their study on USW-aligned embryonic myofibroblasts. However, to the best of our knowledge, no attempt has been made to study the effect of USW alignment on neural cell differentiation.

For our study on neural cell alignment, we employed a moderate input power of 0.45 W, as this provided sufficient acoustic force to direct cell movement to the nodal planes whilst avoiding the onset of acoustic streaming.

Figure 5 shows representative LSCM images of the cells stained with calcein AM (green) and PI (red) 24 h after USW alignment compared to randomly distributed cells in the hydrogel (control). As expected, the USWs gave rise to aligned cell bands within the hydrogel. Similar to the control, most of the USW-aligned cells were stained by calcein AM (green), indicating that the majority of cells remained viable after USW treatment, thus verifying that USW alignment did not produce significant detrimental effects on the cells.

Hydrogels and encapsulated cells were cultured for 7 d to assess the proliferation ability of USW-aligned cells compared to that of non-aligned cells. This was carried out by measuring the DNA content given the strong correlation between the number of cells and the total DNA content. Figure 6 shows that the numbers of USW-aligned and non-aligned cells both gradually increased from day 1 to day 7 ($p < 0.05$, $n = 3$). The proliferation of both USW-aligned and non-aligned cells was slower before day 7. This is not surprising as time is required for the cells to degrade in the surrounding scaffold to make space before they can initiate proliferation. Similar observation has been reported by others who study cell proliferation in other 3D hydrogels [59, 60]. Nonetheless, at each day, no significant differences ($p > 0.05$, $n = 3$) were observed between the two sets of data, indicating that USW treatment did not impede cell growth.

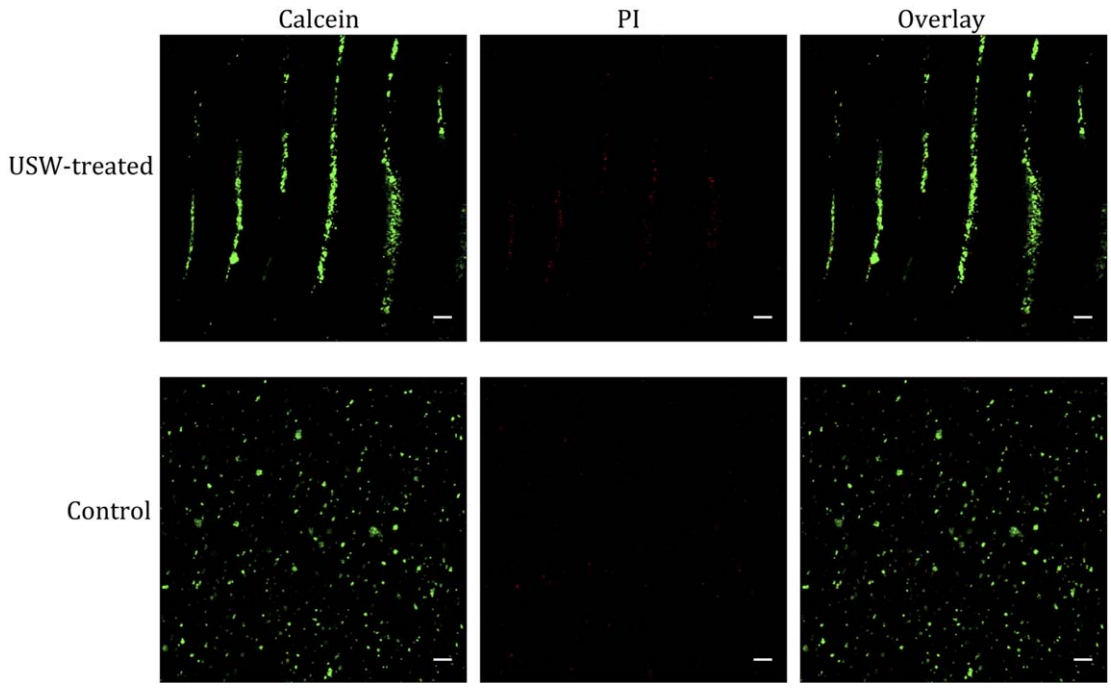

Figure 5. Viability of PC12 cells aligned in 3D hydrogel under USW exposure at 0.45 W, indicated by calcein AM and PI staining, compared to the control in which the cells were not subjected to any acoustic irradiation. The cells were examined 24 h post-USW alignment. The scale bars represent 100 μm.

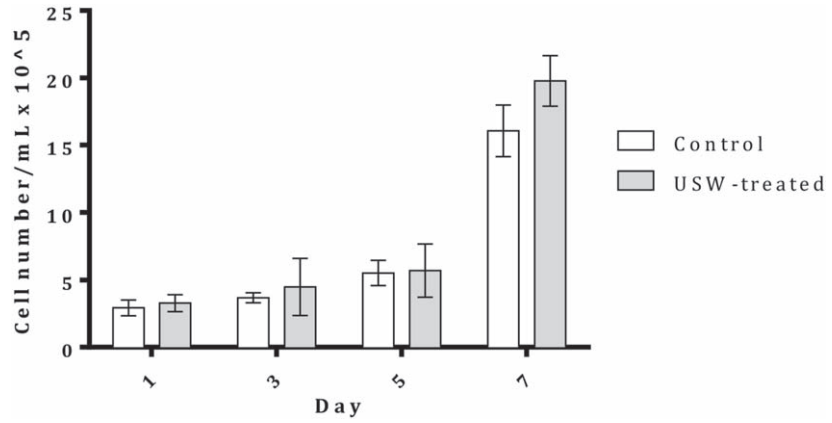

Figure 6. PC12 cell proliferation post-USW treatment, quantified using the PicoGreen® assay. Data are represented as a mean value ± standard deviation ($n = 3$).

3.3. Gene and protein expression

PC12 cells are known to differentiate into neuron-like cells when they are treated with nerve growth factor, which makes them useful as a model to study neuronal differentiation. USW-aligned cells were allowed to differentiate inside hydrogel for 20 d. Neuronal markers targeting different stages of differentiation were examined, i.e. TUBB as an early marker [61], GAP-43 for developing neurons [62], NF-L for mature neurons [63], and Synapsin I for terminally-differentiated neurons [64]. Expression of these markers was expected to be upregulated during the course of PC12 differentiation. Caspr1 was used as a negative marker, as its expression was expected to decrease as the level of myelin protein increased in differentiated PC12 cells [54, 65, 66]. To quantify neuron expression in the differentiated PC12 cells, qPCR was then performed. Figure 7 shows the results for gene expression in USW-aligned cells in terms of the fold change relative to that in differentiated cells without USW treatment. A fold change greater than one thus indicates that the gene expression in USW-treated cells was higher than that in untreated cells within the hydrogel. Generally, all markers showed fold changes greater than one. On Day 15, a small decrease in Caspr1 expression ($p < 0.05$, $n = 3$) and a small increase in TUBB expression ($p < 0.05$, $n = 3$) relative to day ten were observed, suggesting that aligned PC12 cells differentiated slightly faster at the early stages of differentiation culture. No significant difference was observed after

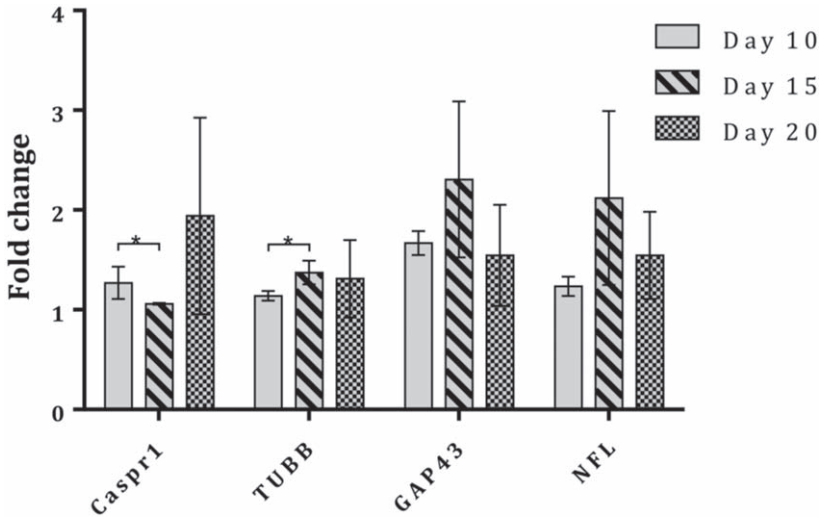

Figure 7. Results from qPCR analysis of differentiated PC12 cells post-USW treatment. The fold changes were calculated relative to differentiated but non-aligned PC12 cells in hydrogel. Data are represented as a mean value ± standard deviation ($^{*}p < 0.05, n = 3$).

20 d of differentiation for both GAP-43 ($p = 0.092$, $n = 3$) and NF-L ($p = 0.089$, $n = 3$), this is probably because given sufficient time, the differentiation of both USW-aligned and untreated PC12 cells has completed, in which the differentiation rate of untreated PC12 cells finally catches up with that associated with cells aligned under USW.

For qualitative analysis, immunostaining was then performed on Day 20 differentiated samples to detect the presence of neuron-specific proteins, namely, β-tubulin, GAP-43, and synapsin I in differentiated PC12 cells embedded in the hydrogel. The morphology of labelled PC12 cells were visualised using confocal microscopy. The representative images in figure 8 show that both USW-treated and untreated cells expressed β-tubulin, GAP-43, and synapsin I markers. Both neurites and cell bodies expressed β-tubulin. The mature and terminal markers, GAP-43 and synapsin I, were found to localise in the cell bodies. This observation together with the results from qPCR analysis confirming that USW treatment did not impede PC12 differentiation.

A difference in neurite growth patterns between the USW-treated and untreated groups was observed from the β-tubulin labelling (figure 8). For USW-treated PC12 cells, the direction of neurite growth was observed to be relatively uniform, whereas the growth direction of neurites in the untreated PC12 cells (control) appeared to be more random. To quantify the alignment of neurites, the angle of neurite orientation with respect to the cell body was measured using ImageJ. As shown in figure 9, the standard deviation of the non-aligned group was significantly higher ($p < 0.05$, $n = 50$), confirming visual observation of neurite orientation. We note that before 20 d, little neurite extension was seen in the 3D hydrogel similar to the that observed by others. For example, Arien-Zalau *et al* [67] observed neurite extension was retarded in the first 15 d when NGF-induced differentiation of PC12 cells was undertaken in a 3D collagen hydrogel. A possible reason for the slow neurite extension is that neurite outgrowth requires the limiting step in which metaloprotease is secreted from PC12 cells to generate sufficient space through proteolytic degradation of the surrounding matrix [67].

Conventional tissue engineering approaches rely on prefabricated topographical or physical microstructures to guide nerve regeneration. In contrast, the present technique provides a means to manipulate cell arrangement and further guide nerve regeneration without requiring lengthy or specialised scaffold prefabrication steps. This finding is promising as it suggests that USW-treated cell-laden hydrogels can potentially be used for peripheral nerve repair.

4. Conclusions

This study successfully demonstrates a simple alternative method to fabricate 3D micropatterned nerve tissues using USWs to align the cells prior to gelation and immobilisation within Gtn-HPA hydrogels. We found that USW irradiation did not reduce cell viability or proliferation ability, nor did it hinder the cells' ability to differentiate when compared to untreated controls. For the first time, we show that axonal growth on differentiated USW-aligned PC12 cells provides greater degree of directional uniformity compared with unaligned cells not exposed to USWs. This promising finding opens up the possibility of exploiting such a system to aid peripheral nerve repair although further *in vivo* testing is required. The simplicity of this technique makes it easy to implement for other tissue engineering applications given that it circumvents the need for expensive and specialised microfabrication equipment.

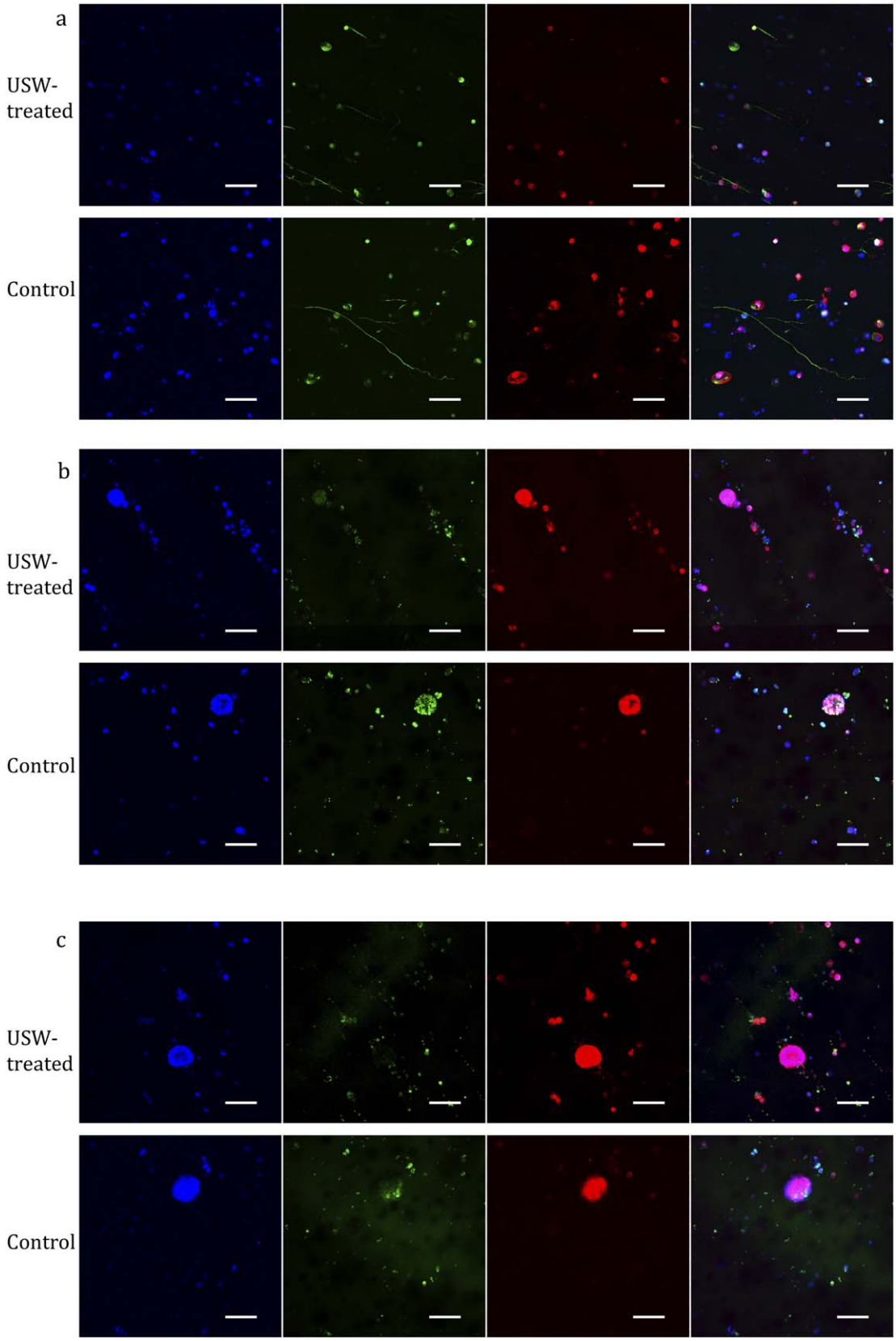

Figure 8. Immunostaining of differentiated PC12 cells on Day 20 of the differentiation. Left to right: DAPI (blue), marker of interest (green), actin (red), overlay. The scale bars represent 200 μm. The markers of interest are (a) β-tubulin, (b) GAP-43, and (c) synapsin I.

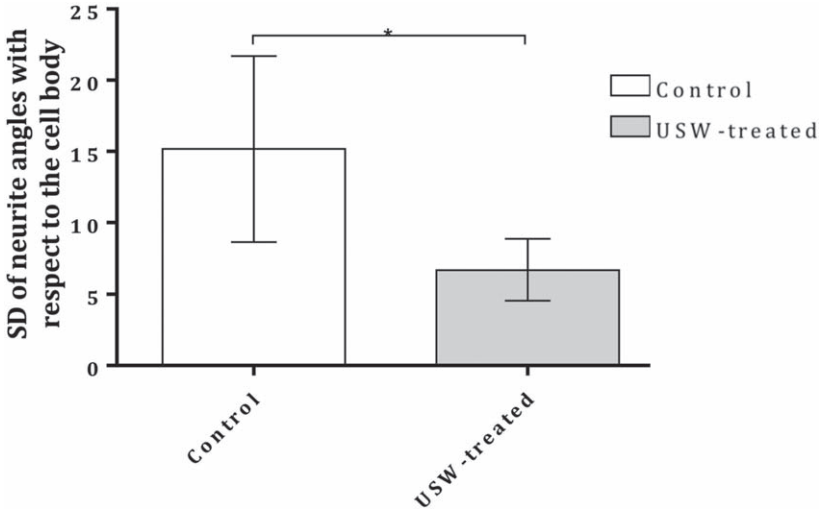

Figure 9. Standard deviation (SD) of neurite angles with respect to the cell body. Data is represented as a mean value ($n = 50$) ± standard deviation ($^{*}p < 0.05, n = 50$).

Acknowledgments

Funding for this work was partly provided through Australian Research Council Discovery Grants DP170103704 and DP160101591.

ORCID iDs

Pauline M Doran https://orcid.org/0000-0002-8682-4929
Leslie Y Yeo https://orcid.org/0000-0002-5949-9729
Peggy P Y Chan https://orcid.org/0000-0001-6676-9769

References

[1] Vinci M, Gowan S, Boxall F, Patterson L, Zimmermann M, Court W, Lomas C, Mendiola M, Hardisson D and Eccles S A 2012 *BMC Biol.* **10** 29
[2] Ravi M, Paramesh V, Kaviya S R, Anuradha E and Solomon F D 2015 *J. Cell. Physiol.* **230** 16–26
[3] Gauvin R, Chen Y C, Lee J W, Soman P, Zorlutuna P, Nichol J W, Bae H, Chen S and Khademhosseini A 2012 *Biomaterials* **33** 3824–34
[4] Triolo D, Dina G, Lorenzetti I, Malaguti M, Morana P, Del Carro U, Comi G, Messing A, Quattrini A and Previtali S C 2006 *J. Cell Sci.* **119** 3981–93
[5] Lee S H, Moon J J and West J L 2008 *Biomaterials* **29** 2962–8
[6] Sorribas H, Padeste C and Tiefenauer L 2002 *Biomaterials* **23** 893–900
[7] Kane R S, Takayama S, Ostuni E, Ingber D E and Whitesides G M 1999 *Biomaterials* **20** 2363–76
[8] Vozzi G, Flaim C, Ahluwalia A and Bhatia S 2003 *Biomaterials* **24** 2533–40
[9] Bertassoni L E, Cardoso J C, Manoharan V, Cristino A L, Bhise N S, Araujo W A, Zorlutuna P, Vrana N E, Ghaemmaghami A M, Dokmeci M R *et al* 2014 *Biofabrication* **6** 024105
[10] Ouyang L, Yao R, Mao S, Chen X, Na J and Sun W 2015 *Biofabrication* **7** 044101
[11] Colosi C, Shin S R, Manoharan V, Massa S, Costantini M, Barbetta A, Dokmeci M R, Dentini M and Khademhosseini A 2016 *Adv. Mater.* **28** 677–84
[12] Roth E A, Xu T, Das M, Gregory C, Hickman J J and Boland T 2004 *Biomaterials* **25** 3707–15
[13] Murphy S V and Atala A 2014 *Nat. Biotechnol.* **32** 773
[14] Ramon-Azcon J *et al* 2012 *Lab Chip* **12** 2959–69
[15] Mohanty S K, Mohanty K S and Berns M W 2008 *J. Biomed. Opt.* **13** 054049
[16] Gosse C and Croquette V 2002 *Biophys. J.* **82** 3314–29
[17] Garvin K A, Hocking D C and Dalecki D 2010 *Ultrasound Med. Biol.* **36** 1919–32
[18] Ozkan M, Pisanic T, Scheel J, Barlow C, Esener S and Bhatia S N 2003 *Langmuir* **19** 1532–8
[19] Deumens R, Bozkurt A, Meek M F, Marcus M A E, Joosten E A J, Weis J and Brook G A 2010 *Prog. Neurobiol.* **92** 245–76
[20] Marquardt L M and Sakiyama-Elbert S E 2013 *Curr. Opin. Biotechnol.* **24** 887–92
[21] Subramanian A, Krishnan U M and Sethuraman S 2009 *J. Biomed. Sci.* **16** 108
[22] Chew S Y, Mi R, Hoke A and Leong K W 2007 *Adv. Funct. Mater.* **17** 1288–96
[23] Kim Y-T, Haftel V K, Kumar S and Bellamkonda R V 2008 *Biomaterials* **29** 3117–27
[24] Schnell E, Klinkhammer K, Balzer S, Brook G, Klee D, Dalton P and Mey J 2007 *Biomaterials* **28** 3012–25
[25] Dinis T M, Elia R, Vidal G, Dermigny Q, Denoeud C, Kaplan D L, Egles C and Marin F 2015 *J. Mech. Behav. Biomed. Mater.* **41** 43–55
[26] Goldner J S, Bruder J M, Li G, Gazzola D and Hoffman-Kim D 2006 *Biomaterials* **27** 460–72
[27] Haq F, Anandan V, Keith C and Zhang G 2007 *Int. J. Nanomed.* **2** 107–15
[28] Petersson F, Nilsson A, Holm C, Jonsson H and Laurell T 2005 *Lab Chip* **5** 20–2
[29] Evander M, Johansson L, Lilliehorn T, Piskur J, Lindvall M, Johansson S, Almqvist M, Laurell T and Nilsson J 2007 *Anal. Chem.* **79** 2984–91
[30] Hawkes J J, Barber R W, Emerson D R and Coakley W T 2004 *Lab Chip* **4** 446–52
[31] Lee Y-H and Peng C-A 2007 *Ultrasound Med. Biol.* **33** 734–42
[32] Coakley W T, Bardsley D W, Grundy M A, Zamani F and Clarke D J 1989 *J. Chem. Technol. Biotechnol.* **44** 43–62
[33] Coakley W T 1997 *Trends Biotechnol.* **15** 506–11
[34] Coakley W T, Hawkes J J, Sobanski M A, Cousins C M and Spengler J 2000 *Ultrasonics* **38** 638–41
[35] Hawkes J J, Barrow D and Coakley W T 1998 *Ultrasonics* **36** 925–31
[36] Kapishnikov S, Kantsler V and Steinberg V 2006 *J. Stat. Mech* P01012-P

[37] Hawkes J J and Coakley W T 2001 *Sensors Actuators* B **75** 213–22
[38] Miles C A, Morley M J, Hudson W R and Mackey B M 1995 *J. Appl. Bacteriol.* **78** 47–54
[39] Ter Haar G and Wyard S J 1978 *Ultrasound Med. Biol.* **4** 111–23
[40] Whitworth G, Grundy M A and Coakley W T 1991 *Ultrasonics* **29** 439–44
[41] Gherardini L, Radel S, Sielemann S, Doblhoff-Dier O, Groschl M, Benes E and McLoughlin A J 2001 *Bioseparation* **10** 153–62
[42] Gherardini L, Cousins C M, Hawkes J J, Spengler J, Radel S, Lawler H, Devcic-Kuhar B, Gröschl M, Coakley W T and McLoughlin A J 2005 *Ultrasound Med. Biol.* **31** 261–72
[43] Garvin K A, Dalecki D, Yousefhussien M, Helguera M and Hocking D C 2013 *J. Acoust. Soc. Am.* **134** 1483–90
[44] Wang L S, Chung J E, Chan P P and Kurisawa M 2010 *Biomaterials* **31** 1148–57
[45] Al-Abboodi A, Fu J, Doran P M, Tan T T Y and Chan P P Y 2014 *Adv. Healthc. Mater.* **3** 725–36
[46] Al-Abboodi A, Tjeung R, Doran P M, Yeo L Y, Friend J and Yik Chan P P 2014 *Adv. Healthc. Mater.* **3** 1655–70
[47] Fon D, Al-Abboodi A, Chan P P Y, Zhou K, Crack P, Finkelstein D I and Forsythe J S 2014 *Adv. Healthc. Mater.* **3** 761–74
[48] Gupta D, Tator C H and Shoichet M S 2006 *Biomaterials* **27** 2370–9
[49] Hoo S P, Sarvi F, Li W H, Chan P P Y and Yue Z 2013 *ACS Appl. Mater. Interfaces* **5** 5592–600
[50] Livak K J and Schmittgen T D 2001 *Methods* **25** 402–8
[51] Liu H X, Zhang J J, Zheng P and Zhang Y 2005 *Brain Res. Mol. Brain Res.* **139** 169–77
[52] Dijkmans T F, van Hooijdonk L W, Schouten T G, Kamphorst J T, Vellinga A C, Meerman J H, Fitzsimons C P, de Kloet E R and Vreugdenhil E 2008 *J. Neurochem.* **105** 2388–403
[53] Schimmelpfeng J, Weibezahn K F and Dertinger H 2004 *J. Neurosci. Methods* **139** 299–306
[54] Lee K-H, Ryu C J, Hong H J, Kim J and Lee E H 2005 *Neurochem. Res.* **30** 533–40
[55] Standley P R, Camaratta A, Nolan B P, Purgason C T and Stanley M A 2002 *Am. J. Physiol. Heart Circ. Physiol.* **283** H1907–14
[56] Standley P R, Camaratta A, Nolan B P, Purgason C T and Stanley M A 2002 *Am. J. Physiol. Heart Circ. Physiol.* **283** H1907
[57] Deck J D 1986 *Cardiovasc Res.* **20** 760–7
[58] Ahmed D, Mao X, Shi J, Juluri B K and Huang T J 2009 *Lab Chip* **9** 2738–41
[59] Liu Y and Chan-Park M B 2010 *Biomaterials* **31** 1158–70
[60] Bott K, Upton Z, Schrobback K, Ehrbar M, Hubbell J A, Lutolf M P and Rizzi S C 2010 *Biomaterials* **31** 8454–64
[61] Long X, Olszewski M, Huang W and Kletzel M 2005 *Stem. Cells Dev.* **14** 65–9
[62] Turner J H, May L, Reed R R and Lane A P 2010 *Am. J. Rhinol. Allergy* **24** 192–6
[63] Lariviere R C and Julien J-P 2004 *J. Neurobiol.* **58** 131–48
[64] Thiel G, Greengard P and Südhof T C 1991 *Proc. Natl Acad. Sci. USA* **88** 3431–5
[65] Einheber S, Zanazzi G, Ching W, Scherer S, Milner T A, Peles E and Salzer J L 1997 *J. Cell Biol.* **139** 1495–506
[66] Scherer S S 1999 *Ann. New York Acad. Sci.* **883** 131–42
[67] Arien-Zakay H, Lecht S, Perets A, Roszell B, Lelkes P I and Lazarovici P 2009 *J. Mol. Neurosci.* **37** 225–37